Microtubules with a twist: a lumenal interrupted helix in human sperm tail microtubules

John Heumann*, Cindi L. Schwartz*, Azusa Suzuki-Shinjo**, Garry Morgan*, Per Widlund***, Johanna Höög****

* Department of Molecular, Cellular and Developmental Biology, University of Colorado, Boulder, CO, USA

** Krefting Research Centre, University of Gothenburg, Gothenburg, Sweden

*** Sahlgrenska Academy, University of Gothenburg, Gothenburg, Sweden

**** Department of Chemistry and Molecular Biology, University of Gothenburg, Gothenburg, Sweden

Corresponding author: johanna.hoog@gu.se

Keywords: spermatozoa, cryo-electron tomography, microtubules, flagella, cilia, singlet region, microtubule associated protein, human

Abstract

The microtubule cytoskeleton, important for cell division and motility, is regulated by a complex system of microtubule-associated proteins and motors. Microtubule inner proteins (MIPs) are a novel group of Microtubule associated proteins (MAPs) that are localized inside the microtubule lumen. Previously, known MIPS consisted of single proteins or small protein complexes.

The tips of flagella possess a region containing only singlet microtubules. We have examined this singlet zone in intact human sperm tails by cryo-electron tomography followed by subvolume averaging and report the presence of a novel structure on the interior of the microtubules that we call: “TAILS” (Tail Axoneme Intra-Lumenal Spirals). This structure spans the entire singlet zone (several micrometers) and forms a left-handed interrupted helix with 8 nm rise and 12 nm pitch. TAILS is coaxial with the surrounding microtubule helix, which is consistent with identical subunits binding directly to the interior microtubule wall but leaves a gap over the microtubule seam.

This is the first higher order structure found inside of a microtubule lumen. We suggest that TAILS may stabilize microtubules, enable rapid swimming, or play a role in controlling the direction in which spermatozoa swim.

Introduction

Microtubules are essential for many cellular functions including maintenance of cell shape, segregation of chromosomal DNA during division, and cellular motility. They are dynamic structures that repeatedly undergo cycles of growth and shrinkage (Mitchison & Kirschner, 1984); however, their dynamics varies greatly *in vivo*. Microtubules in mitotic spindles are highly dynamic (Needleman *et al*, 2010), while those in the *Trypanosoma brucei* microtubule cytoskeleton are extremely stable (Robinson *et al*, 1991). In comparison, microtubules reconstituted *in vitro* from pure tubulin (Bowne-Anderson *et al*, 2013) have intermediate dynamicity. Therefore, differences in microtubule dynamics must be tightly regulated by factors in the cellular environment.

Hundreds of microtubule-associated proteins (MAPs) and motor proteins are known to be involved in the regulation of the microtubule cytoskeleton (Nogales & Zhang, 2016; Howard & Hyman, 2007; Akhmanova & Steinmetz, 2015). MAPs fall into several categories based on their functions, but with regards to localization, there are three main types: those that bind the more dynamic plus end (+TIPs, e.g. EB1, XMAP215 and Clip170;(Perez *et al*, 1999; Mimori-Kiyosue *et al*, 2000; Nakaseko *et al*, 2001), those that bind and often stabilize the minus end (e.g. gamma tubulin and patronin;(Goodwin & Vale, 2010; Kollman *et al*, 2010; Oakley & Oakley, 1989), and those that more generally interact with the microtubule outer surface (e.g. PRC1; (Chan *et al*, 1999; Kellogg *et al*, 2016)). Motor proteins can also be found at all three locations, depending on the polarity of their movement (Scheffler *et al*, 2015). Altogether, in any given cell, the microtubule outer surfaces, plus, and minus ends are often occupied by a wide assortment of MAPs and motor proteins that affect their characteristics, likely exerting effects in synergistic ways (Teng *et al*, 2001; Zanic *et al*, 2013). Only two known MAPs, tau and tubulin acetylase, have been suggested to localize to the microtubule interior (Kar *et al*, 2003; Soppina *et al*, 2012). Until recently, the microtubule lumen has not been the focus of investigations into MAPs influence on microtubules.

Electron microscopy, and (cryo-)electron tomography in particular, has shown that proteins also localize to the inside of microtubules (Nicastro, 2006; Schwartz *et al*, 2012; Dentler, 1980; Rodríguez Echandía *et al*, 1968; Vaughan *et al*, 2006; Höög *et al*, 2007; Garvalov *et al*, 2006; Sui & Downing, 2006). These microtubule inner proteins (MIPs) that have been observed are all of unknown protein identity and function. While protein identity has not yet been determined for any MIP, their specific localization and variable frequency suggests that they serve important regulatory functions for the microtubule cytoskeleton (Nicastro *et al*, 2011). Previously described MIPs have been separate proteins or small protein complexes on the inside of microtubule lattice. Here we reveal a novel protein complex spanning several micrometers in the lumens of human spermatozoa axonemal microtubules.

Materials and methods

Sample collection and plunge freezing

Sperm was donated by three healthy men and frozen unperturbed in seminal fluid to which colloidal gold was added (to be used as fiducial markers). A Vitrobot climate-controlled plunge freezer (FEI Company Ltd., Eindhoven, The Netherlands) was used within 1-3 hours post ejaculation. After freezing for electron microscopy, remaining cells were examined under the light microscope, where their motility ensured that viable spermatozoa had been frozen.

Cryo-electron microscopy and tomography

Microscopy was performed as described previously (Höög *et al*, 2012; Höög & Lötvall, 2015). In brief, images (electron dose of ~25 $e^-/Å^2$; -4-6 μm defocus) were acquired at 27500x on a Tecnai F30 electron microscope (FEI Company Ltd) operated at 300 kV. The detector was a GATAN UltraCam, lens-coupled, 4 K CCD camera (binned by 2) attached to a Tridiem Gatan Image Filter (GIF: operated at zero-loss mode with an energy window of 20 eV; Gatan Inc., Pleasanton, CA, USA). For tomography, tilt-series were acquired every 1.5 degree (±60 degrees) using serialEM software (Mastronarde, 2005). The total electron dose was kept between 80-120 $e^-/Å^2$.

Subvolume Alignment, Averaging, and Statistical Analysis

Models with open contours approximating the path of each microtubule were created in IMOD (Kremer *et al*, 1996). Addition of model points with the desired spacing (ultimately, 8 nm) along each contour and subsequent alignment and averaging of 60 $voxel^3$ (46.2 nm^3) subvolumes centered on each point were done using PEET (Nicastro, 2006). 1940 subvolumes from 3 sperm tails containing a total of 34 singlet microtubules were analyzed. Subvolumes from individual microtubules were first aligned and averaged separately. Final alignment and averaging combining microtubules and tomograms was then performed starting from positions and orientations obtained by aligning the individual tube averages. Soft-edge cylindrical masks with empirically chosen radii were applied during alignment. Wedge-mask compensated principal component analysis followed by k-means clustering (Heumann *et al*, 2011) was used to check for heterogeneity and to assess the impact of missing wedge artifacts on candidate alignments.

Results

An interrupted helix in the singlet microtubule lumen

Motile eukaryotic flagella, such as sperm tails, consist of two central pair microtubules surrounded by nine doublet microtubules (Fisch & Dupuis-Williams, 2011). The doublet microtubules consist of a complete A-tubule and an incomplete B-tubule. Close to the distal tip of the flagellum, the B-tubule often terminates and the A-tubule continues forming “the singlet zone” (Ringo, 1967; Satir, 1968). However, the presence of this singlet zone and its extent vary greatly (Höög *et al*, 2014), for example in rodent sperm, both the A- tubule and the B-tubule from a doublet microtubule transition into singlet microtubules at the flagellum tip (Woolley & Nickels, 1985).

We performed cryo-electron microscopy of the distal tip of human spermatozoa plunge frozen in complete seminal fluid, and found an extensive singlet zone. Inside the singlet microtubules, a striation was noticed (Figure 1A; Supplementary figure 1; n=23 sperm tips). To investigate this striation further, we generated 55 cryo-electron tomograms of intact human sperm tails. The exact location and area included in 24 of those tomograms could be identified using lower magnification images along the sperm tails (Figure 1B).

The end piece of spermatozoa contained only singlet microtubules (Figure 1C). Cryo-tomogram slices through the microtubule lumen display an unexpected, extensive, and regular interior structure in all microtubules (Figure 1D). Transverse lumenal slices offset from the center display diagonal striations with 8 nm periodicity. The tilt of the striations reverses on opposing sides of the lumen (arrows and Supplementary movie 1), suggesting a left-handed helix with a pitch of 8 nm. It is, however, difficult to see how one might reconcile an 8 nm pitch interior helix with the 12 nm pitch and seam expected for 13

protofilament microtubule walls. To resolve this discrepancy and clarify the nature of the structure, we performed subvolume alignment and averaging of 1940 particles found along 34 singlet microtubules.

Fine structure of the Tail Axoneme Intra-lumenal Spiral (TAILS) complex

Subvolume averaging increased the single-to-noise ratio revealing a left-handed interrupted helix. In cross-sectional view an internal density is clearly visible (Figure 2A) which rotates around the lumen when viewed at successive positions along the microtubule axis (Supplemental movie 2). In longitudinal view, the helix is clearly recognizable as the repetitive pattern seen in the raw data (Figure 1D-F and Figure 2B-H; Supplemental Movie 3). A 3D model of the sub-tomogram average was created using density thresholding, which also showed the helical structure of the MIP (Figure 2I-J; Supplemental Movie 4). We named this structure "TAILS" (Tail Axoneme Intra-Lumenal Spirals).

A TAILS complex occurs every 8 nm along the microtubule axis (Figure 2C and F), each segment has a pitch of 12 nm, matching that of 13 the protofilament microtubule wall. 13 protofilament microtubules consist of a 3-start helix with α and β tubulin subunits laterally adjacent to subunits of the same type (a B-lattice) except at a "seam", where α tubulin is adjacent to β tubulin (an A-lattice, Figure 3A) (McIntosh *et al*, 2009; Kikkawa *et al*, 1994). This led us to examine the site of TAILS binding in relation to the microtubule seam, which could be identified in the subtomogram average (Figure 3B; Supplementary Figure 2).

The TAILS complex follows the tubulin helix but leaves a gap at the microtubule seam

Moving through the sub-tomogram average, gaps in the TAILS complexes are apparent on the inside of the microtubule (Figure 3C; Supplementary movie 2). Each segment spans between 240 and 305 degrees (based on centers or edges of electron densities, respectively) leaving a gap spanning portions of 2-3 protofilaments around the seam (Figure 3C-D). The proximal end of a given segment occurs at approximately the same axial height as the distal end of the previous segment (Figure 3C; white arrows). The result is a stack of identically oriented, C-shaped segments coaxial with the surrounding tubulin helix (Figure 3E). This stack can also be thought of as an interrupted or incomplete 3-start helix.

The TAILS complex span the entire micrometer-long singlet region

Previously known microtubule-associated structures have usually localized to a small area of that microtubule, for example the microtubule tip. To investigate the extent of the TAILS complex, cryo-electron tomograms further from the tip were examined. Approximately 2.5 µm from the tip, there is a transition between singlet microtubules and doublet microtubules (Figure 4A-B). In this region, the TAILS complex is still continuous inside all the singlet microtubules, terminating approximately 300 nm into the doublet MT (Figure 4C). The TAILS structure thus spans close to 3 µm in the spermatozoon end pieces. Nearer the cell body, the A-tubule is filled with an amorphous electron density, but the B-tubule remains electron translucent and the 8 nm periodicity associated with the TAILS helix continues further inside the B-tubule.

While the termination patterns of individual microtubules are variable, the central pair microtubules ends 7.16 µm from the cell tip in one tomogram. Here, the doublet microtubules have been helix free for several micrometers. However, the TAILS helix is found in the terminal part of the central pair (Figure 5).

Discussion

This is the first time an intact human flagellum has been studied using cryo-electron tomography. We have described a novel TAILS structure in which helical segments spaced every 8 nm and jointly spanning several micrometers line the lumen of all singlet microtubules in the end piece of human sperm tails. To our knowledge, the TAILS structure represents the most extensive, highly organized structure reported within a microtubule lumen to date. The function of this structure is of course of highest interest. We suggest three different hypotheses, which are not mutually exclusive. 1) TAILS might provide extra rigidity to the microtubules in this region, so that the end piece has an increased stiffness, which would aid rapid motility, crucial to spermatozoa. It may provide a structural support such as the para-flagellar rod in *Trypanosoma brucei* (Höög *et al*, 2012; Portman & Gull, 2010), another single cell whose motility is crucial for its survival (Broadhead *et al*, 2006). 2) The TAILS complex could also stabilize microtubules, preventing the dynamic growing and shortening constantly occurring in flagella tips (Marshall, 2001). Helical reinforcement is a low weight solution regularly used in engineering, *e.g.* in bicycle frame tubes or in armored hoses. Since microtubules depolymerize by outward curling of protofilaments (Simon & Salmon, 1990; Mandelkow *et al*, 1991), TAILS could prevent splaying similar to how spiral hose reinforcement prevents radial expansion. The saved energy could then instead be invested in rapid translocation. This hypothesis is consistent with the observation that the TAILS complexes extend to the central pair microtubules, far into the sperm tail. 3) TAILS might also play a role in determining the direction in which spermatozoa swim, since in other organisms, there is evidence that the singlet zone may be associated with signaling / sensory function as well as motility (Fisch & Dupuis-Williams, 2011).

TAILS have a pitch and handedness matching that of the tubulin helices comprising the microtubule wall. This pattern is consistent with what would be expected for a structure comprised of repeating identical subunits capable of distinguishing between α and β tubulin. For example, the putative inner wall-binding monomers might bind preferentially to either α tubulin, β tubulin, the α-β groove, or the β-α groove. We are presently unable to distinguish between these possibilities; however, we note that there is ample precedent among motor domains and other proteins which bind microtubules externally with such specificity, such as kinesin, dynein and PRC1 who all bind the tubulin intradimer interface (Kellogg *et al*, 2016; Redwine *et al*, 2012; Gigant *et al*, 2013).

Potential mechanisms for controlling the extent and orientation of the helical segments are worth considering. The TAILS complex has a gap in the structure spanning the inside of the microtubule seam. Binding specificity of the putative inner wall binding monomers coupled with conformational variation of the subunits closest to the seam alone could account for the observed structure. A monomer specific for inner wall β tubulin, for example, would be unable to bind to the α tubulin subunit across the seam, leaving a gap. If a bridge over this gap is present, such a structure would likely be comprised of protein(s) distinct from the inner wall binding monomers, and its length might naturally limit the span of the helical segments.

The finding of a novel, complex structure inside of the microtubule lumen, despite having been studied for over 50 years, underlines the importance of studying human microtubules and flagella, as well as other organisms, by electron tomography. Since sperm motility and morphology are determinants of male fertility (Esteves, 2016), understanding the functional role of the TAILS complex may have clinical implications relating to male infertility and contraception. We look forward to the future identification of

the proteins involved in regulating the microtubule cytoskeleton from the lumenal side, including the proteins forming the TAILS complex.

Acknowledgements

We thank Dr. J. Van Blerkom at Colorado Reproductive Endocrinology for providing samples for our study, and J. R. McIntosh and A. Hoenger for helpful discussions. JHL was supported by a Sir Henry Wellcome Postdoctoral grant, a VR young investigator grant and the Göran Gustafsson Foundation for Research in Natural Sciences and Medicine. Electron microscopy was done at Boulder EM Services Core Facility in MCDB, the University of Colorado.

Author contribution

Experimental design: JLH, POW. Acquisition of cryo-electron micrographs: JLH, GM. Acquisition of cryo-electron tomograms: JLH, CLS. Calculation and modelling of tomograms: JLH. Subtomogram averaging and processing of data: JH, ASS. Writing of manuscript: JH, POW and JLH.

Figure legends:

Figure 1: Microtubules in the end piece of the human spermatozoon show a repetitive pattern inside their lumen A) A cryo-electron micrograph of one sperm tail tip showing repetitive decoration of microtubules (zoomed image). B) A drawing illustrating positions along the sperm tail where cryo-electron tomograms were acquired. D) A 15 nm thick slice from a cryo-electron tomogram of a sperm end piece showing singlet microtubules with repetitive diagonal striations with variable tilt directions (arrows). E-F) 7 nm thick slices of individual singlet microtubules from the sperm end piece in D.

Figure 2: Subtomogram averaging reveals the repetitive pattern inside the microtubule lumen to be an interrupted left-handed helix, or stacks of helical segments, that follows the pattern of the internal microtubule lattice. A) A 0.7 nm thick cross-sectional view of the subtomogram average, showing the microtubule and the internal electron density (green arrow). B-H) 0.7 nm thick longitudinal slices through the subtomogram average showing the microtubule lattice in B) and H). One turn of the helix is highlighted with green on top of the electron densities inside of the microtubule lumen in C-G. I) The 3D model shows the microtubule lattice (turquoise) and the intralumenal structure (green). Longitudinal view of the sub-tomogram average. J) One side of protofilament has been cut away from the model to reveal the internal helical structure.

Figure 3: The TAILS complex forms a gap over the microtubule seam. A) Cartoon of a typical 13 protofilament microtubule with the 3 start helix and a 12 nm pitch. The microtubule seam is marked with the red dotted line. B) A slice of the sub-tomogram average shows a disruption in the microtubule B-lattice, revealing the location of the seam (red cross). C) Cross-sectional view of the subtomogram average showing the end of one TAILS complex segment and the beginning of the next. D) 3D model of the microtubule (turquoise) and the TAILS complex (green) reveals the gap (yellow arrow) of the TAILS complex. E) A schematic of a 13 protofilament microtubule opened up into a sheet. The TAILs complex (green) is placed at an arbitrary position along the y-axis, as we do not know the exact location.

Figure 4: The TAILS complex span the entire singlet region A) A tomographic slice showing the area of the sperm tail where the doublet microtubules end and the singlet microtubules protrude. B) A 3D model of the sperm tail showing the membrane in brown, the A-tubules in turquoise and the B-tubules in blue. C) A tomographic slice showing the end of the TAILS complex (white arrows) inside the doublet microtubule.

Figure 5: The TAILS complex is also present in the terminal parts of the central pair microtubules, ~7 micrometer from the sperm tip. A) Slice from an cryo-electron tomogram showing the distal ends of the central pair microtubules. B-C) Zoomed in images of the central pair microtubules show the typical striations of the TAILs complex.

Supplementary material:

Supplementary figure 1: Cryo-EM of three intact human spermatozoa's distal tip (end piece) derived from three different donors. In all three the repetitive pattern inside the microtubules in the singlet region is clearly visible. The arrows point to some of the more apparent places, but the helical pattern is present through most, if not all, visible areas.

Supplementary figure 2: The location of the microtubule seam. A) A top-down view of the 3D average of the microtubule, including the helix, sub-tomogram average. Arbitrary numbers have been given to protofilaments to correlate to the images in B and C. B) Slices of the sub-tomogram average oriented such that two neighboring protofilaments are visualized. The red cross is the location of the red ball in C). The purple line shows the slope between neighboring tubulin subunits and fits all protofilament pairs except for pair 12-13 where no tubulin subunits could be identified, and pair 13-1 where the slope between protofilaments are different (green line) showing that the seam is here. C) A longitudinal view of the microtubule 3D model and the protofilaments.

Supplementary movies:

Movie 1: The microtubule singlet region of the intact human spermatozoon. All microtubules have a complete decoration of the TAILS complex.

Movie 2: Cross-sectional view of the microtubule subtomogram average and the electron densities that is the TAILS complex that rotates around the lumen. 6 frames/s. Scale bar 10 nm.

Movie 3: Longitudinal view of the microtubule subtomogram average containing the TAILS complex. 6 frames/s. Scale bar 10 nm.

Movie 4: 3D model of the subtomogram average showing the microtubule lattice in turquoise and the TAILS complex in green. 15 frames/s.

References

Akhmanova A & Steinmetz MO (2015) Control of microtubule organization and dynamics: two ends in the limelight. *Nat Rev Mol Cell Biol* **16:** 711–726

Bowne-Anderson H, Zanic M, Kauer M & Howard J (2013) Microtubule dynamic instability: A new model with coupled GTP hydrolysis and multistep catastrophe. *Bioessays* **35:** 452–461

Broadhead R, Dawe HR, Farr H, Griffiths S, Hart SR, Portman N, Shaw MK, Ginger ML, Gaskell SJ, McKean PG & Gull K (2006) Flagellar motility is required for the viability of the bloodstream trypanosome. *Nature* **440:** 224–227

Chan J, Jensen CG, Jensen LC, Bush M & Lloyd CW (1999) The 65-kDa carrot microtubule-associated protein forms regularly arranged filamentous cross-bridges between microtubules. *Proc. Natl. Acad. Sci. U.S.A.* **96:** 14931–14936

Dentler WL (1980) Structures linking the tips of ciliary and flagellar microtubules to the membrane. *J. Cell. Sci.* **42:** 207–220

Esteves SC (2016) Novel concepts in male factor infertility: clinical and laboratory perspectives. *Journal of Assisted Reproduction and Genetics***:** 1–17

Fisch C & Dupuis-Williams P (2011) Ultrastructure of cilia and flagella - back to the future! *Biology of the Cell* **103:** 249–270

Garvalov BK, Zuber B, Bouchet-Marquis C, Kudryashev M, Gruska M, Beck M, Leis A, Frischknecht F, Bradke F, Baumeister W, Dubochet J & Cyrklaff M (2006) Luminal particles within cellular microtubules. *J. Cell Biol.* **174:** 759–765

Gigant B, Wang W, Dreier B, Jiang Q, Pecqueur L, Plückthun A, Wang C & Knossow M (2013) Structure of a kinesin–tubulin complex and implications for kinesin motility. *Nature Publishing Group* **20:** 1001–1007

Goodwin SS & Vale RD (2010) Patronin Regulates the Microtubule Network byProtecting Microtubule Minus Ends. *Cell* **143:** 263–274

Heumann JM, Hoenger A & Mastronarde DN (2011) Journal of Structural Biology. *J. Struct. Biol.* **175:** 288–299

Howard J & Hyman AA (2007) Microtubule polymerases and depolymerases. *Current Opinion in Cell Biology* **19:** 31–35

Höög JL & Lötvall J (2015) Diversity of extracellular vesicles in human ejaculates revealed by cryo-electron microscopy. *Journal of Extracellular Vesicles* **4:**

Höög JL, Bouchet-Marquis C, McIntosh JR, Hoenger A & Gull K (2012) Cryo-electron tomography and 3-D analysis of the intact flagellum in Trypanosoma brucei. *J. Struct. Biol.* **178:** 189–198

Höög JL, Lacomble S, O'Toole ET, Hoenger A, McIntosh JR & Gull K (2014) Modes of flagellar assembly in Chlamydomonas reinhardtii and Trypanosoma brucei. *eLife* **3:** e01479

Höög JL, Schwartz C, Noon AT, O'Toole ET, Mastronarde DN, McIntosh JR & Antony C (2007) Organization of interphase microtubules in fission yeast analyzed by electron tomography. *Dev. Cell* **12:** 349–361

Kar S, Fan J, Smith MJ, Goedert M & Amos LA (2003) Repeat motifs of tau bind to the insides of microtubules in the absence of taxol. *EMBO J.* **22:** 70–77

Kellogg EH, Howes S, Ti S-C, Ramírez-Aportela E, Kapoor TM, Chacón P & Nogales E (2016) Near-atomic cryo-EM structure of PRC1 bound to the microtubule. *Proceedings of the National Academy of Sciences* **113:** 9430–9439

Kikkawa M, Ishikawa T, Nakata T, Wakabayashi T & Hirokawa N (1994) Direct visualization of the microtubule lattice seam both in vitro and in vivo. *J. Cell Biol.* **127:** 1965–1971

Kollman JM, Polka JK, Zelter A, Davis TN & Agard DA (2010) Microtubule nucleating γ-TuSC assembles structures with 13-fold microtubule-like symmetry. *Nature* **466:** 879–882

Kremer JR, Mastronarde DN & McIntosh JR (1996) Computer visualization of three-dimensional image data using IMOD. *J. Struct. Biol.* **116:** 71–76

Mandelkow EM, Mandelkow E & Milligan RA (1991) Microtubule dynamics and microtubule caps: a time-resolved cryo-electron microscopy study. *J. Cell Biol.* **114:** 977–991

Marshall WF (2001) Intraflagellar transport balances continuous turnover of outer doublet microtubules: implications for flagellar length control. *J. Cell Biol.* **155:** 405–414

Mastronarde DN (2005) Automated electron microscope tomography using robust prediction of specimen movements. *J. Struct. Biol.* **152:** 36–51

McIntosh JR, Morphew MK, Grissom PM, Gilbert SP & Hoenger A (2009) Lattice Structure of Cytoplasmic Microtubules in a Cultured Mammalian Cell. *Journal of Molecular Biology* **394:** 177–182

Mimori-Kiyosue Y, Shiina N & Tsukita S (2000) The dynamic behavior of the APC-binding protein EB1 on the distal ends of microtubules. *Curr. Biol.* **10:** 865–868

Mitchison T & Kirschner M (1984) Dynamic instability of microtubule growth. *Nature* **312:** 237–242

Nakaseko Y, Goshima G, Morishita J & Yanagida M (2001) M phase-specific kinetochore proteins in fission yeast: microtubule-associating Dis1 and Mtc1 display rapid separation and segregation during anaphase. *Curr. Biol.* **11:** 537–549

Needleman DJ, Groen A, Ohi R, Maresca T, Mirny L & Mitchison T (2010) Fast microtubule dynamics in meiotic spindles measured by single molecule imaging: evidence that the spindle environment does not stabilize microtubules. *Mol. Biol. Cell* **21:** 323–333

Nicastro D (2006) The Molecular Architecture of Axonemes Revealed by Cryoelectron Tomography. *Science* **313:** 944–948

Nicastro D, Fu X, Heuser T, Tso A, Porter ME & Linck RW (2011) Cryo-electron tomography reveals conserved features of doublet microtubules in flagella. *Proc. Natl. Acad. Sci. U.S.A.* **108:** E845–53

Nogales E & Zhang R (2016) ScienceDirectVisualizing microtubule structural transitions and interactions with associated proteins. *Current Opinion in Structural Biology* **37:** 90–96

Oakley CE & Oakley BR (1989) Identification of gamma-tubulin, a new member of the tubulin superfamily encoded by mipA gene of Aspergillus nidulans. *Nature* **338:** 662–664

Perez F, Diamantopoulos GS, Stalder R & Kreis TE (1999) CLIP-170 highlights growing microtubule ends in vivo. *Cell* **96:** 517–527

Portman N & Gull K (2010) The paraflagellar rod of kinetoplastid parasites: From structure to components and function. *International Journal for Parasitology* **40:** 135–148

Redwine WB, Hernández-López R, Zou S, Huang J, Reck-Peterson SL & Leschziner AE (2012) Structural basis for microtubule binding and release by dynein. *Science* **337:** 1532–1536

Ringo DL (1967) Flagellar motion and fine structure of the flagellar apparatus in Chlamydomonas. *J. Cell Biol.* **33:** 543–571

Robinson D, Beattie P, Sherwin T & Gull K (1991) Microtubules, tubulin, and microtubule-associated proteins of trypanosomes. *Meth. Enzymol.* **196:** 285–299

Rodríguez Echandía EL, Piezzi RS & Rodríguez EM (1968) Dense-core microtubules in neurons and gliocytes of the toad Bufo arenarum Hensel. *Am. J. Anat.* **122:** 157–166

Satir P (1968) Studies on cilia. 3. Further studies on the cilium tip and a 'sliding filament' model of ciliary motility. *J. Cell Biol.* **39:** 77–94

Scheffler K, Minnes R, Fraisier V, Paoletti A & Tran PT (2015) Microtubule minus end motors kinesin-14 and dynein drive nuclear congression in parallel pathways. *J. Cell Biol.* **209:** 47–58

Schwartz CL, Heumann JM, Dawson SC & Hoenger A (2012) A Detailed, Hierarchical Study of Giardia lamblia's Ventral Disc Reveals Novel Microtubule-Associated Protein Complexes. *PLoS ONE* **7:** e43783

Simon JR & Salmon ED (1990) The structure of microtubule ends during the elongation and shortening phases of dynamic instability examined by negative-stain electron microscopy. *J. Cell. Sci.* **96 (Pt 4):** 571–582

Soppina V, Herbstman JF, Skiniotis G & Verhey KJ (2012) Luminal Localization of α-tubulin K40 Acetylation by Cryo-EM Analysis of Fab-Labeled Microtubules. *PLoS ONE* **7:** e48204

Sui H & Downing KH (2006) Molecular architecture of axonemal microtubule doublets revealed by cryo-electron tomography. *Nature* **442:** 475–478

Teng J, Takei Y, Harada A, Nakata T, Chen J & Hirokawa N (2001) Synergistic effects of MAP2 and MAP1B knockout in neuronal migration, dendritic outgrowth, and microtubule organization. *J. Cell Biol.* **155:** 65–76

Vaughan S, Shaw M & Gull K (2006) A post-assembly structural modification to the lumen of flagellar microtubule doublets. *Curr. Biol.* **16:** R449–50

Woolley DM & Nickels SN (1985) Microtubule termination patterns in mammalian sperm flagella. *J.*

Ultrastruct. Res. **90:** 221–234

Zanic M, Widlund PO, Hyman AA & Howard J (2013) ncb2744. *Nat Cell Biol* **15:** 688–693

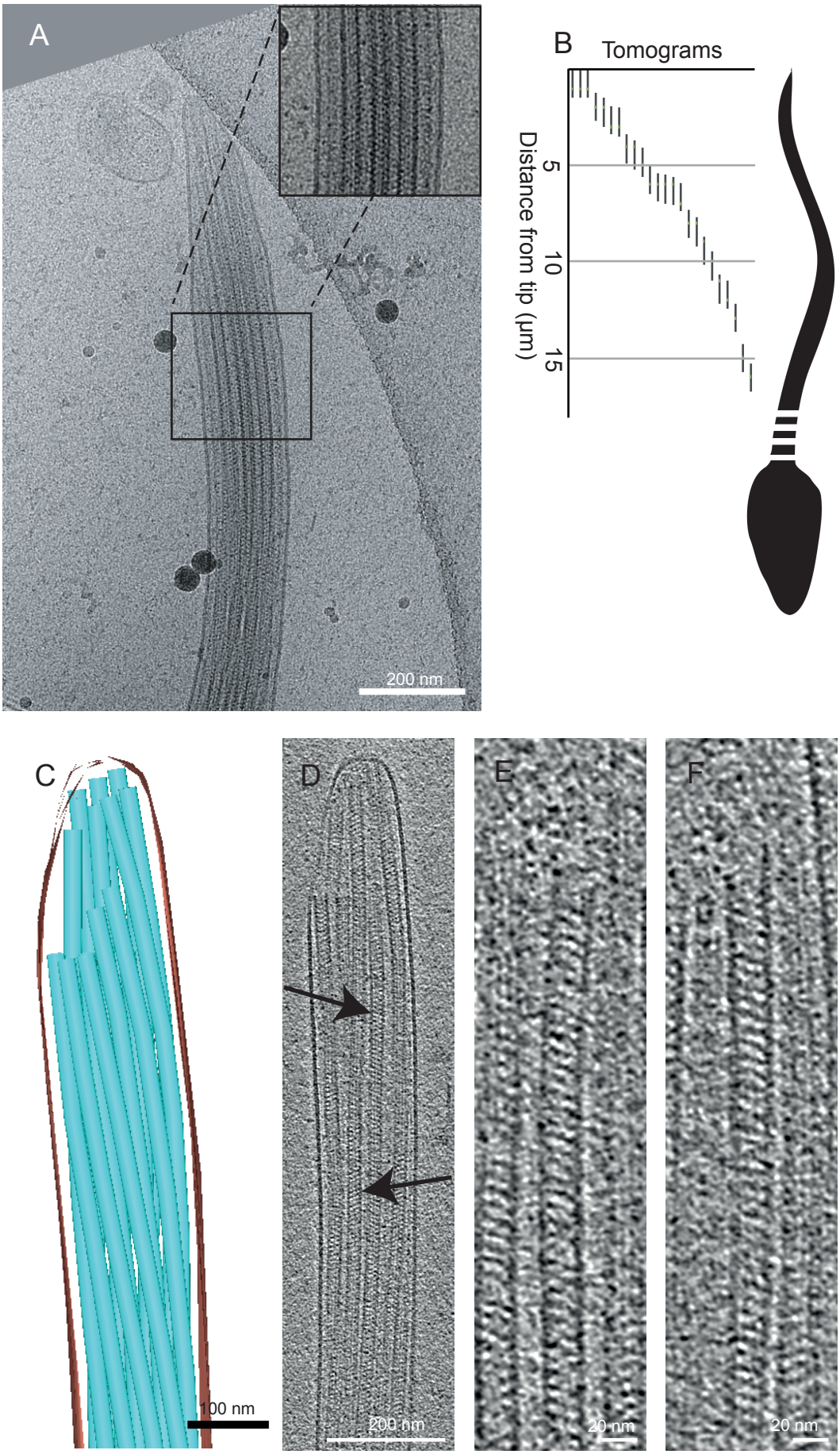
A
200 nm
B
Tomograms
Distance from tip (µm)
5
10
15
C
100 nm
D
200 nm
E
20 nm
F
20 nm

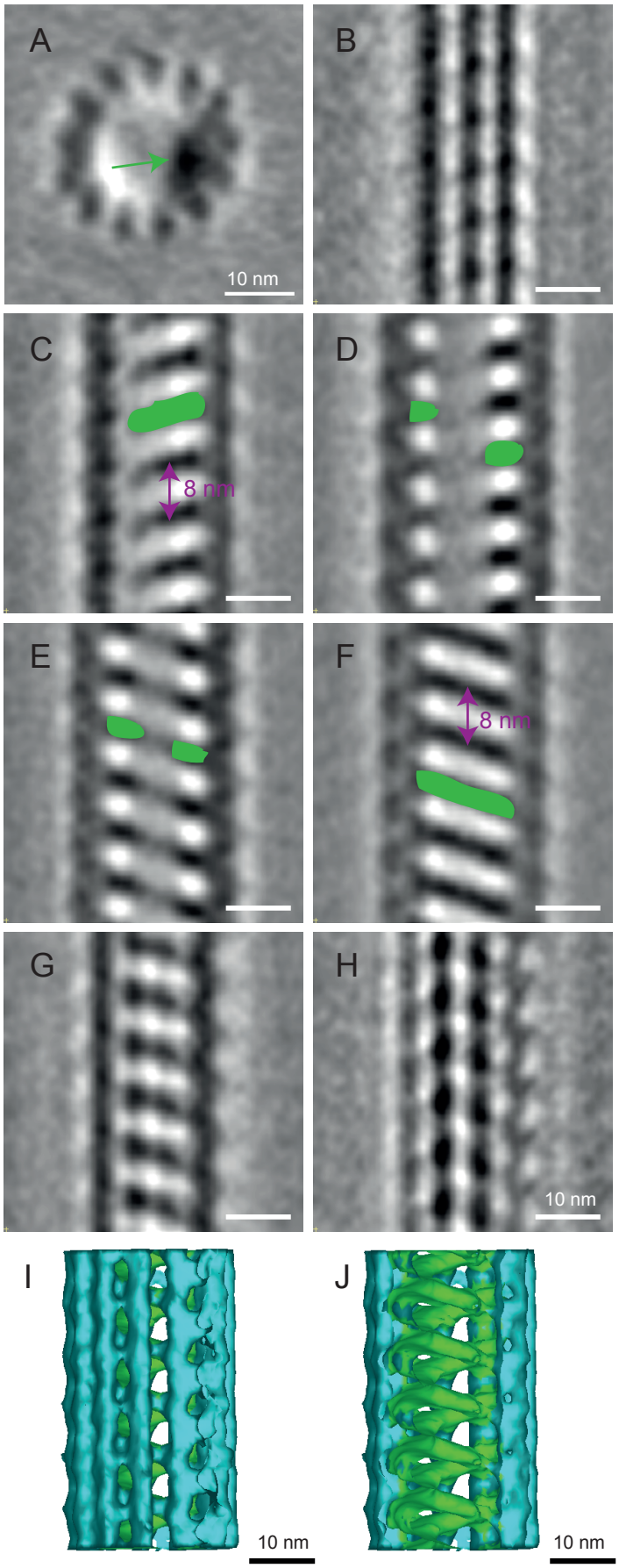
A
10 nm
B
C
8 nm
D
E
F
8 nm
G
H
10 nm
I
10 nm
J
10 nm

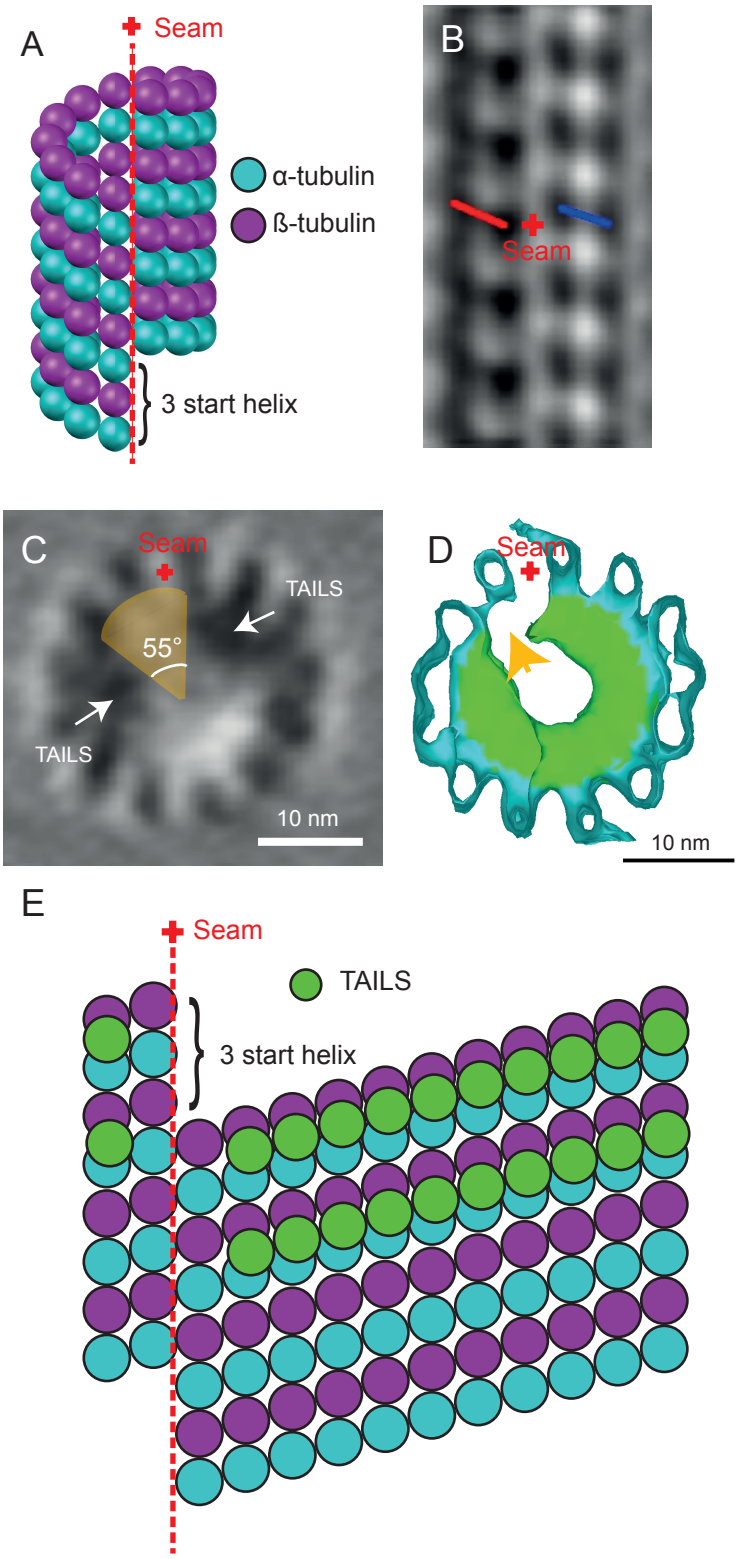
A
Seam
α-tubulin
ß-tubulin
3 start helix
B
Seam
C
Seam
TAILS
55°
TAILS
10 nm
D
Seam
10 nm
E
Seam
TAILS
3 start helix

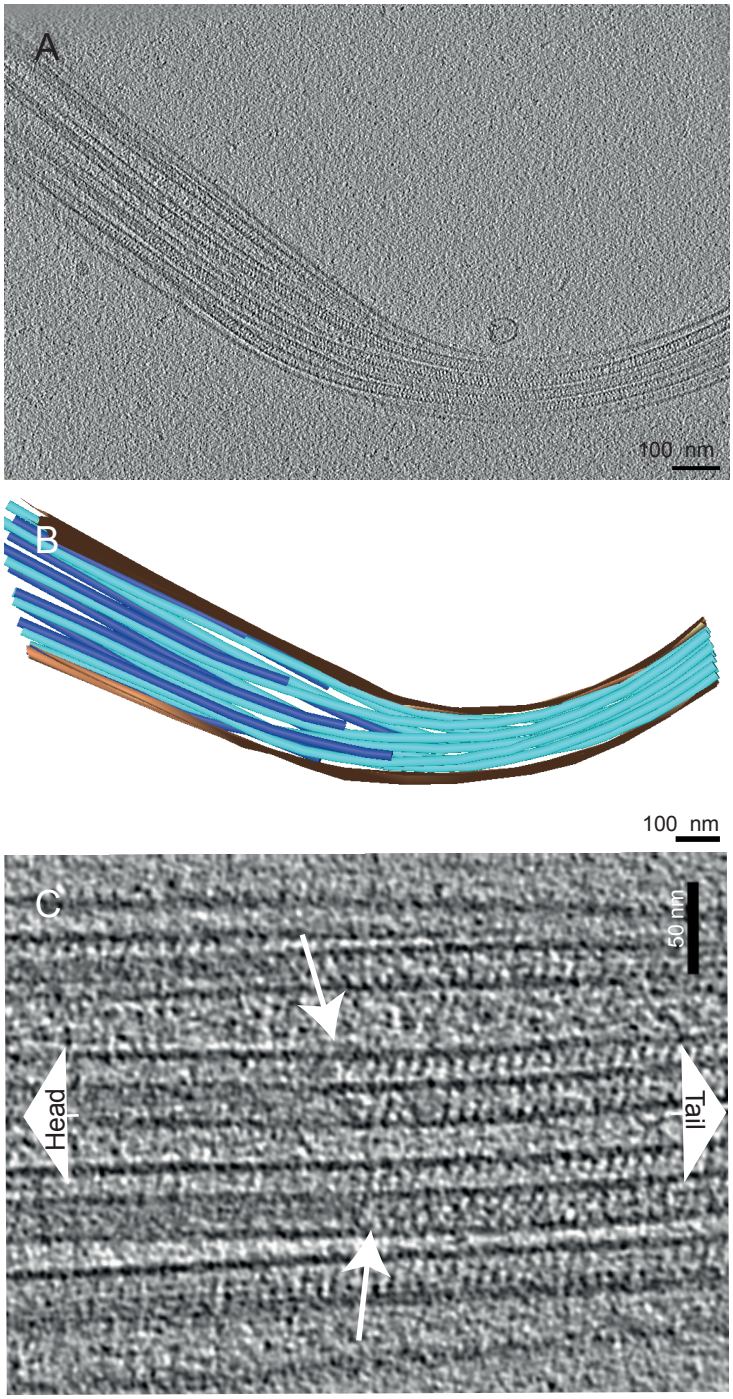
A
100 nm
B
100 nm
C
50 nm
Head
Tail

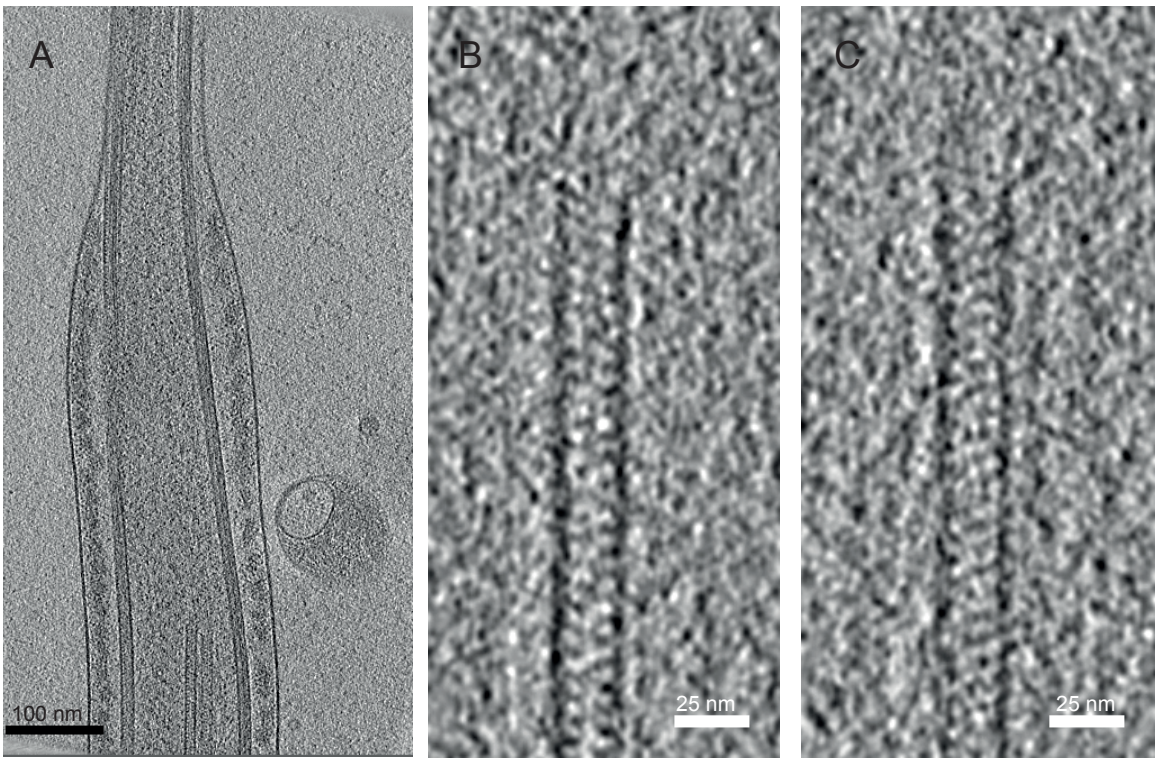
A
100 nm
B
25 nm
C
25 nm